LOCALLY STRUCTURED LOW-RANK MR IMAGE RECONSTRUCTION USING SUBMATRIX CONSTRAINTS

Xi Chen, Wenchuan Wu, Mark Chiew

Wellcome Center for Integrative Neuroimaging, FMRIB, Nuffield Department of Clinical Neurosciences, University of Oxford, Oxford, United Kingdom

ABSTRACT

Image reconstruction methods based on structured low-rank matrix completion have drawn growing interest in magnetic resonance imaging. In this work, we propose a locally structured low-rank image reconstruction method which imposes low-rank constraints on submatrices of the Hankel structured k-space data matrix. Simulation experiments based on numerical phantoms and experimental data demonstrated that the proposed method achieves robust and significant improvements over the conventional, global structured low-rank methods across a variety of structured matrix constructions, sampling patterns and noise levels, at the cost of slower convergence speed only.

Index Terms— Structured low-rank, locally low-rank

1. INTRODUCTION

Structured low-rank (SLR) methods have become increasingly popular for MRI reconstruction problems, particularly for under-sampled image recovery. These methods have been successfully employed in many applications such as phase-constrained imaging [1], calibration-less parallel imaging reconstruction [2, 3], multi-shot EPI reconstruction [4], EPI Nyquist ghost correction [5]. SLR methods are typically based on Hankel structured low-rank matrix completion and provide a powerful framework that offers great flexibility to exploit different forms of linear dependency in MR data to constrain image reconstruction. More specifically, the Hankel-structured matrix generated in SLR methods usually consists of a single or multiple concatenated block-Hankel matrix representations of k-space data, with low-rank properties arising from annihilation relations in the spatial-frequency domain [6, 7].

The low-rank matrices in SLR methods can be constructed in a number of different ways, e.g., the C-matrix, S-matrix [1], or "Virtual Coil Hankel matrix" (VC-matrix) [8, 9], and similarly their low-rank properties can be enforced in various ways, e.g., strict rank constraint or nuclear norm minimization. However, what all existing methods share in common is global enforcement of the low-rank property on the Hankel-structured matrix. In contrast to globally low-rank constraints, locally low-rank (LLR) methods have been developed for various constrained reconstruction problems [10]. However, to our knowledge, while LLR constraints have been developed for image-space regularisation, they have not yet been explored for k-space SLR problems.

In this paper, we propose a new non-convex SLR matrix recovery method, termed locally structured low-rank (LSLR), which enforces low-rank constraints on submatrices of the Hankel structured matrix. The LSLR penalty is sufficiently flexible to work with virtually any conventional SLR matrix construction. Specifically, we partition the matrix into disjoint submatrices prior to independently constraining the rank of each one, within an alternating direction method of multipliers iterative optimization algorithm [11]. To prevent submatrix boundary artifacts, we employ a cycle-spinning approach to shift submatrix boundaries randomly every iteration.

The rest of the paper is organized as follows: Section 2 describes the LSLR penalty formulation in detail along with one possible implementation, and experiment methods used to evaluate its performance; Section 3 shows the experiment results and Section 4 concludes the paper.

2. METHODS

2.1. LSLR Formulation

Without loss of generality, we consider a simple 2D reconstruction problem as a representative example, with straightforward extension to higher dimensional problems. Consider the non-convex SLR reconstruction problem formulated as follows:

$$\hat{X} = \underset{X}{\operatorname{argmin}} \|EX - Y\|^2 \quad s.t. \; rank(H_c X) = r \tag{1}$$

Where $X \in \mathbb{C}^{n^2 N_c}$ corresponds to the k-space data of a $n \times n$ image with N_c channels, and the forward measurement model E represents the sampling operator S: $\mathbb{C}^{n^2 N_c} \rightarrow \mathbb{C}^{N_k N_c}$ which selects the same N_k k-space samples from each channel. $Y \in \mathbb{C}^{N_k N_c}$ denotes the acquired k-space data so that the under-sampling factor is defined as N_k/n^2. Here we

define a basic Hankel transform operator $H: \mathbb{C}^{n^2} \to \mathbb{C}^{l\times d^2}$, assuming its kernel size to be $d \times d$, and that $l = (n - d + 1)^2$. The Hankel structured matrix is constructed by vertically concatenating row-vectors corresponding to all $d \times d$ patches of k-space. The augmented operator $H_c: \mathbb{C}^{n^2 N_c} \to \mathbb{C}^{l\times d^2 N_c}$ horizontally concatenates the Hankel transform of multiple channels along the column dimension. Note typically the number of rows l of $H_c X \gg$ its number of columns $d^2 N_c$. The rank parameter $r \ll \min(l, d^2 N_c)$, and here we use a non-convex strict rank constraint to enforce the low-rank property on the Hankel matrix $H_c X$.

The conventional SLR approach enforces the low-rank property on the full Hankel-structured matrix, which corresponds to a single set of null space vectors (or equivalently annihilating filters) for the Hankel-structured matrix. In contrast, the proposed LSLR method formulates the reconstruction as:

$$\hat{X} = \underset{X}{\operatorname{argmin}} \|EX - Y\|^2 \qquad (2)$$
$$s.t. rank(\Gamma_i H_c X) = r, \quad \forall \Gamma_i \in \Omega = \{\Gamma_1, \Gamma_2, \dots, \Gamma_m\}$$

Where $\Gamma_i: \mathbb{C}^{l\times d^2 N_c} \to \mathbb{C}^{s\times d^2 N_c}$ is the operator that selects $s = l/m$ consecutive rows from the Hankel matrix to form the i^{th} submatrix, and the adjoint operator $\Gamma_i^*: \mathbb{C}^{s\times d^2 N_c} \to \mathbb{C}^{l\times d^2 N_c}$ places the submatrix rows back at their original positions with all other row vectors being 0. Note when l/m is not an integer, s is typically rounded to be the smallest integer close to it for simplicity. $\Gamma_i \in \Omega$, where Ω is the set of m operators selecting all the non-overlapping submatrices of $H_c X$, so that Γ_1 selects the rows of index $1{:}\, s$ and Γ_2 selects rows of index $s + 1{:}\, 2s$, etc. Thus, when $m = 1$ and $s = l$, LSLR reconstruction is exactly the same as SLR reconstruction. As the submatrices select a subset of row vectors of the Hankel matrix, each of them should still be of low-rank as long as $s > d^2 N_c$. This formulation relaxes the single rank constraint over $H_c X$ to a set of constraints on m disjoint submatrices.

In this work, the optimization problems for SLR and LSLR are both solved by the alternating direction method of multipliers (ADMM) [11] algorithm which reformulates the optimization as:

$$\min_{X,Z,W} \|EX - Y\|_2^2 + \rho \|H_c X - Z + W\|_2^2 \qquad (3)$$
$$s.t. rank(\Gamma_i Z) = r, \quad \forall \Gamma_i \in \Omega = \{\Gamma_1, \Gamma_2, \dots, \Gamma_m\}$$

To promote shift-invariance and avoid potential boundary artifacts, we employ a cycle-spinning procedure by randomly shifting the positions of the submatrices between [1, l] at every iteration of the ADMM algorithm [12]. Thus, a different set Ω_j is chosen at the j_{th} iteration. The proposed approach can also be viewed as a stochastic algorithm that iterates over randomly chosen subsets of all possible $s \times d^2 N_c$ submatrices. Details of the algorithm are shown in Table 1. Note that SLR is represented as a special case of LSLR when $m = 1$, except that a fixed Ω is used at every iteration.

Step 1. initialize $X_0 = Y,\ Z_0 = H_c X_0, W_0 = 0, j = 0$
Step 2. solve subproblem a, b, c alternately a. Update X_{j+1} by solving: $min\|EX - Y\|^2 + \lambda\|H_c X - Z_j + W_j\|^2$ Solution: $X_{j+1} = \left(E^* E + \lambda H_c{}^* H_c\right)^{-1}(E^* Y + \lambda H_c{}^*(Z_j - W_j))$ b. Update Z_{j+1} by solving: $min\|H_c X_{j+1} - Z + W_j\|_2^2$ $s.t.\ \ rank(\Gamma_i Z) = r \quad \forall \Gamma_i \in \Omega_j$ Solution: 1) Generate Ω_j, and then for each $\Gamma_i \in \Omega_j$ Calculate SVD decomposition: $U_i \Sigma_i V_i' = SVD(\Gamma_i(H_c X_{j+1} + W_j))$ Perform hard threshold truncation on Σ_i so that $\sigma_k = 0$ if $k > r$, where σ_k *is the* k_{th} largest singular value along the diagonal of Σ_i 2) $Z_{j+1} = \sum_{\Gamma_i \in \Omega_j} \Gamma_i^*(U_i \Sigma_i V_i')$ c. Update W_{j+1}: $W_{j+1} = H_c X_{j+1} - Z_{j+1} + W_j$
Step 3. Set $j = j + 1$, repeat Step 2 until a prescribed number of iteration or a stopping criterion is reached

Table 1 Algorithm for solving SLR/LSLR.

2.2. Experimental Methods

An 80×80 Shepp-Logan numerical phantom with smooth, random phase was used as ground truth for numerical simulations. Partial Fourier sampling with 75% under-sampling factor was simulated. Varying amount of complex Gaussian noise ($s.d. = \{0,1,3,6,9\} \times 10^{-3}$ relative to maximum k-space energy) was added to the k-space data. SLR and LSLR reconstructions based on S-matrix [1] style Hankel-structured matrices were compared.

Another two experiments were based on experimental 128×128 GRE data with 8 synthetic channels (compressed from 32-channel source data for computational efficiency), where 1) 2D random sampling (50.4%); 2) uniform under-sampling (50.8% by skipping every other line while preserving the two central lines) with additional 3/4 partial Fourier (total under-sampling 38.3%) were performed retrospectively. SLR and LSLR reconstructions were based on the C-matrix [1] and VC-matrix [8, 9], for which Hankel matrices constructed from the original k-space and conjugate symmetric k-space of multiple channels are concatenated along the column dimension, using the same phase constraints as the S-matrix under a different construction.

A 128×128 T1w dataset with 8 compressed channels was also used for validation, where 1D random under-sampling (45.3%) was simulated. SLR and LSLR reconstruction based on S-matrix were performed.

Reconstruction fidelity was evaluated using:

$$NRMSE(X) = \|X - X_{gt}\|_2^2 / \|X_{gt}\|_2^2 \qquad (4)$$

Where X and X_{gt} are the reconstructed and ground truth images. For the experimental data, we used the fully-sampled reconstruction as a proxy for the ground truth. The ADMM penalty parameter ρ were 10^{-10} and 10^{-4}, and the kernel size of the Hankel operator were 9×9 and 5×5 for the numerical phantom and experimental data respectively. The rank parameter r was hand tuned to produce the lowest NRMSE for SLR and the same rank was used for LSLR. The number of submatrices for LSLR reconstruction is specified as in LSLR(m). The reconstruction code is available at https://github.com/XChen-p/Locally-Structured-Low-Rank.

3. RESULTS

Fig. 1 shows the reconstruction results based on the S-matrix formulation of the numerical Shepp-Logan phantom with $s.d. = 10^{-3}$ Gaussian noise. The LSLR(4) achieves lower NRMSE than SLR reconstruction. Table 2 compares the SLR and LSLR reconstruction results of the numerical phantom datasets with varying Gaussian noise, where LSLR reconstructions outperform SLR reconstructions across $s.d. = \{0,1,3,6\} \times 10^{-3}$, and they achieve comparable NRMSE at $s.d. = 9 \times 10^{-3}$.

Fig. 2 and Fig.3 show the reconstruction results based on the C-matrix and VC-matrix of the GRE data, where two different sampling patterns were used. In both cases, the LSLR reconstructions converge to lower NRMSE than the SLR reconstruction with more iterations.

Fig. 4 shows the comparison between SLR and LSLR reconstructions based on S-matrix on the T1w dataset, where the LSLR reconstruction also has better performance than the SLR reconstruction. The computation times for SLR and LSLR(4) were 36 and 54 minutes respectively for 3000 iterations.

4. CONCLUSION AND DISCUSSION

In this work, we proposed the LSLR matrix recovery method, which outperforms global SLR matrix recovery across a variety of low-rank matrix constructions (C-matrix, S-matrix and VC-matrix), sampling patterns and noise levels. Unlike the SLR method which enforces low-rank constraint on the entire Hankel structured matrix, the LSLR method relaxes this by instead imposing the low-rank constraints on submatrices of the Hankel structured matrix. While we chose to demonstrate LSLR with ADMM optimization here, it would be straightforward to implement this method within other optimization schemes. Also, although the optimal number of submatrices of LSLR is data-dependent, a simple choice of 2 or 4 could lead to a robust improvement over SLR.

One potential reason why LSLR has better performance over SLR is that the relaxed low-rank constraints on submatrices can achieve more flexibility by allowing for variations in the null-space vectors. While some shift invariant annihilation filters (e.g. due to limited support or smooth phase) have been theoretically justified for MR data, other, shift-variant low-rank properties of the Hankel structured matrix might also be contributing here. Meanwhile, the cycle-spinning procedure can still encourage common null space vectors across the entire Hankel matrix, promoting global low-rank structure. Further validation is needed to understand the mechanism of improvement of local over global structured low-rank methods. In practice, the variations of annihilation filters for different spatial frequency components may also be advantageous when time-dependent sampling considerations are significant, such as in long, single-shot acquisition schemes like echo-planar imaging.

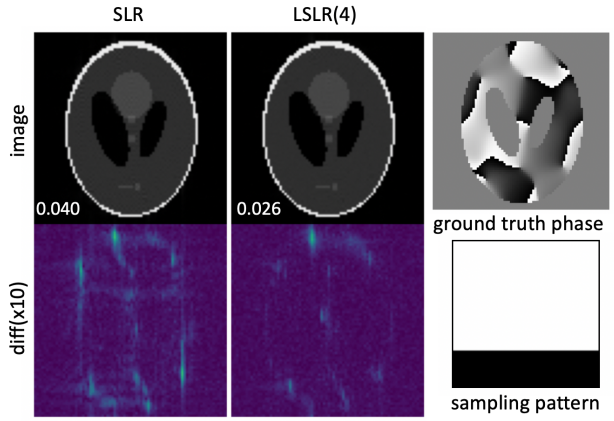

Fig. 1. Reconstruction results based on the S-matrix formulation of the numerical phantom with partial Fourier under-sampling. The reconstructed images with NRMSE values (top) and their differences compared to the ground truth (bottom) of SLR (left) and LSLR (right) reconstructions are shown. The ground truth image phase and sampling pattern are also shown. $r = 130$ was used.

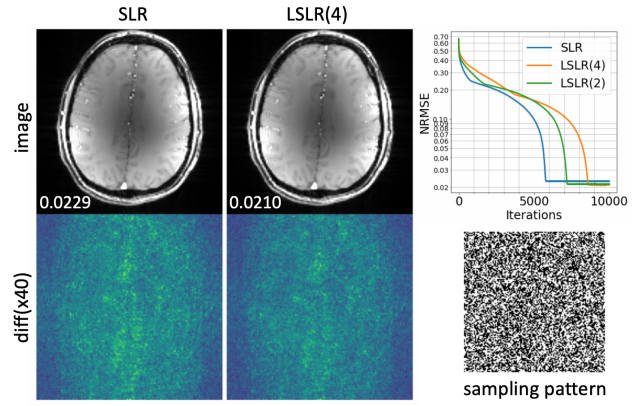

Fig. 2. Results based on the C-matrix formulation of the GRE data with random under-sampling. The reconstructed images with NRMSE values (top) and their differences compared to the ground truth (bottom) of SLR (left) and LSLR (right) reconstructions are shown. $r = 120$ was used.

s.d. of noise	0	10^{-3}	3×10^{-3}	6×10^{-3}	9×10^{-3}
SLR	0.020	0.040	0.062	0.098	0.137
LSLR	**0.013**	**0.026**	**0.050**	**0.094**	**0.136**

Table 2. Normalized RMSE of reconstruction results of the numerical phantom data with varying Gaussian noise**.** The noise amplitude is indicated by its standard deviation relative to the maximum k-space energy. LSLR reconstructions with 2 submatrices were used at $s.d. = 9 \times 10^{-3}$ and 4 submatrices were used for all other datasets. $r = 130$ was used for $s.d. = \{0,1\} \times 10^{-3}$, $r = 120$ was used for $s.d. = \{3,6\} \times 10^{-3}$ and $r = 110$ was used for $s.d. = 9 \times 10^{-3}$.

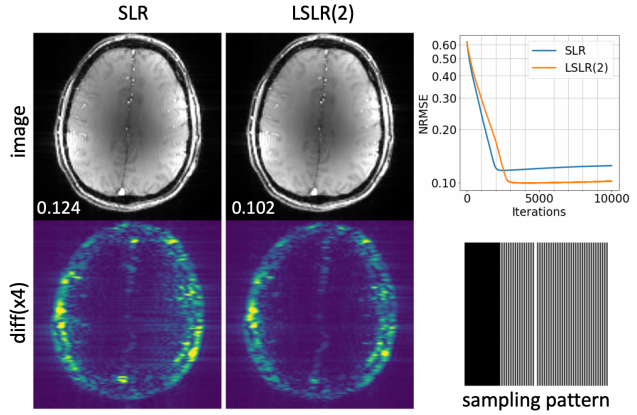

Fig. 3. Results based on the VC-matrix of the GRE data. The reconstructed images with NRMSE values (top) and their corresponding differences compared to the ground truth (bottom) of SLR (left) and LSLR(2) (right) are shown. $r = 180$ was used.

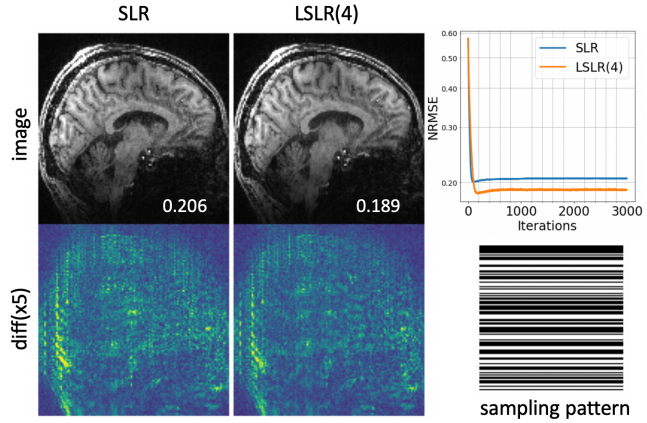

Fig. 4. Results based on the S-matrix of the T1w data. The reconstructed images with NRMSE values (top) and their corresponding differences compared to the ground truth (bottom) of SLR (left) and LSLR(4) (right) are shown. $r = 140$ was used.

5. COMPLIANCE WITH ETHICAL STANDARDS

The experimental data was acquired in accordance with local ethics.

6. ACKNOWLEDGMENTS

The Wellcome Centre for Integrative Neuroimaging is supported by core funding from the Wellcome Trust (203139/Z/16/Z). MC and WW are supported by the Royal Academy of Engineering (RF201617\16\23, RF201819\18\92).

7. REFERENCES

[1] Haldar, J.P., Low-rank modeling of local k-space neighborhoods (LORAKS) for constrained MRI. IEEE Trans Med Imaging, 2014. 33(3): p. 668-81.
[2] Haldar, J.P. and Zhuo, J., P-LORAKS: Low-rank modeling of local k-space neighborhoods with parallel imaging data. Magn Reson Med, 2016. 75(4): p. 1499-514.
[3] Shin, P.J., et al., Calibrationless parallel imaging reconstruction based on structured low-rank matrix completion. Magn Reson Med, 2014. 72(4): p. 959-70.
[4] Mani, M., et al., Multi-shot sensitivity-encoded diffusion data recovery using structured low-rank matrix completion (MUSSELS). Magn Reson Med, 2017. 78(2): p. 494-507.
[5] Lee, J., Jin, K.H. and Ye, J.C., Reference-free single-pass EPI Nyquist ghost correction using annihilating filter-based low rank Hankel matrix (ALOHA). Magn Reson Med, 2016. 76(6): p. 1775-1789.
[6] Jacob, M., Mani, M.P. and Ye, J.C., Structured Low-Rank Algorithms: Theory, Magnetic Resonance Applications, and Links to Machine Learning. IEEE Signal Processing Magazine, 2020. 37(1): p. 54-68.
[7] Haldar, J.P. and Setsompop K. Linear predictability in magnetic resonance imaging reconstruction: Leveraging shift-invariant Fourier structure for faster and better imaging. IEEE Signal Processing Magazine, 2020. 37(1): p.69-82.
[8] Kim, T.H. and Haldar, J.P., LORAKS software version 2.0: Faster implementation and enhanced capabilities. University of Southern California, Los Angeles, CA, Tech. Rep. USC-SIPI-443, 2018.
[9] Bilgic, B., et al. Robust high-quality multi-shot EPI with low-rank prior and machine learning. in Proc Int Soc Magn Reson Med. 2019.
[10] Trzasko, J.D. and Manduca A., Calibrationless parallel MRI using CLEAR. in 2011 conference record of the forty fifth Asilomar conference on signals, systems and computers (ASILOMAR). 2011. IEEE.
[11] Boyd, S., Distributed Optimization and Statistical Learning via the Alternating Direction Method of Multipliers. Foundations and Trends® in Machine Learning, 2010. 3(1): p. 1-122.
[12] Saucedo, A., et al., Improved computational efficiency of locally low rank MRI reconstruction using iterative random patch adjustments. IEEE transactions on medical imaging, 2017. 36(6): p. 1209-1220.